Grain Size Constraints on Glacial Circulation in the Southwest Atlantic

Peter T. Spooner[1], David J. R. Thornalley[1], and Philip Ellis[1]

[1] Department of Geography, University College London, UK.

Corresponding author: Peter T. Spooner (p.spooner@ucl.ac.uk)

Key Points:

- The Vema Channel is a key location for monitoring past changes in deep-Atlantic flow speed.
- We use sortable silt mean grain size analyses to update work using silt mean grain size and assess glacial Antarctic Bottom Water flow.
- Northward flow of Antarctic Bottom Water through the Vema Channel was likely more vigorous during the glacial period.

Abstract

Knowledge of past deep-ocean current speeds has the potential to inform our understanding of changes in the climate system on glacial-interglacial timescales, because they may be used to help constrain changes in deep-ocean circulation rates and pathways. Of particular interest is the paleo-flow speed of southern-sourced deep-water, which may have acted as a carbon store during the last glacial period. A location of importance in the northward transport of southern-sourced bottom water is the Vema Channel, which divides the Argentine and Brazil basins in the South Atlantic. We revisit previous studies of paleo-flow in Vema Channel using updated techniques in grain size analysis (i.e. mean sortable silt grain size), in Vema Channel cores and cores from the Brazil margin. Furthermore, we update the interpretation of the previous grain size studies in the light of many years further research into the glacial circulation of the deep Atlantic. Our results are broadly consistent with the existing data and suggest that during the last glacial period there was slightly more vigorous intermediate to mid-depth (shallower than 2600 m) circulation in the South Atlantic Ocean than in the Holocene, whereas below 3500 m the circulation was generally more sluggish. Increased glacial flow speed on the eastern side of the Vema Channel was likely related to an increase in northward velocity of AABW in the channel. An increase in Antarctic Bottom Water flow through the Vema Channel may have helped to sustain the large volume of southern-sourced deep-water in the Atlantic during the glacial period.

1 Introduction

During the Last Glacial Maximum (LGM) the Atlantic Ocean had an abrupt chemocline at ~2500 m, suggesting a shoaling of the boundary between northern- and southern-sourced water, with the latter filling much of the deep Atlantic (Curry & Oppo, 2005; Hodell et al., 2003; Lynch-Stieglitz et al., 2007). $\delta^{18}O$ and $\delta^{13}C$ constraints suggest that this ocean state was maintained by either a decrease in mixing between Antarctic Bottom Water (AABW) and overlying water, an increase in the formation and transport rates AABW, or a combination of the two (Hoffman & Lund, 2012; Lund, Adkins & Ferrari, 2011). A decrease in mixing likely occurred due to shoaling of the boundary between the deep and shallow overturning cells above rough topography, and intense salinification of the deep water (Adkins, McIntyre & Schrag, 2002; Ferrari et al., 2014; Hoffman & Lund, 2012). However, direct evidence constraining glacial AABW volume transport and/or production is limited, preventing an assessment of its potential role in the altered ocean circulation, carbon cycling and climate state of the LGM.

Reconstructions of glacial $\delta^{13}C$ and $\Delta^{14}C$ suggest that the deep ocean was more poorly ventilated than today (Burke & Robinson, 2012; Hodell et al., 2003; Skinner et al., 2015). Deep waters in the Atlantic were very depleted in radiocarbon, though bottom waters were relatively enriched (but still more depleted than today) (Barker et al., 2010; Burke et al., 2015; Skinner et al., 2010). These observations suggest quite vigorous AABW production during the LGM. However, quantifying glacial-interglacial changes in AABW strength from $\Delta^{14}C$ records is complicated by: 1) changes in water mass mixing; and 2) unquantified changes in air-sea gas exchange - driven by changes in temperature, Southern Ocean stratification and sea-ice extent. Glacial $^{231}Pa/^{230}Th$ evidence suggests reduced deep-Atlantic southwards export, in comparison to vigorous export in the 'glacial north-Atlantic intermediate water' (GNAIW) (Gherardi et al., 2009; Negre et al., 2010), although recent modern studies have drawn attention to the difficulty of using $^{231}Pa/^{230}Th$ as an AMOC proxy (Hayes et al., 2015). Sortable silt mean grain size (SS) and $\delta^{13}C$ data from the eastern New Zealand margin suggest an increase in glacial deep western boundary current (DWBC) flow speed and AABW production (Hall et al., 2001), while Pa/Th and SS data from the Indian Ocean suggest little change in AABW flow between the glacial period and the Holocene (Mccave et al., 2005; Thomas, Henderson & McCave, 2007). In addition, models can reproduce a volumetric expansion of AABW without any recourse to an increase in its formation rate (De Boer & Hogg, 2014). Similarly, it has been suggested that this volumetric increase can explain a significant part of the glacial-interglacial change in atmospheric CO_2 without a change in the rate of bottom water formation (Skinner, 2009). More records of bottom water paleo-flow speed would help to address the mixed findings of the above studies, and inform understanding of glacial-interglacial climate.

A useful location in which to study changes in Atlantic AABW flow is the Vema Channel (39.5^{o}W, 30^{o}S). In the South Atlantic, AABW flows northwards via the Rio Grande Rise, where it must flow through the Vema Channel, the Hunter Channel or over the Santos Plateau (Fig. 1). The Vema Channel is the most important of these conduits, 400 km long and up to 4550 m deep, with ~4 Sv of northward flow through the deep channel (McDonagh, Arhan & Heywood, 2002;

Speer et al., 1993). It is also the only conduit deep enough to transport Weddell Sea Deep Water (WSDW) (Jungclaus & Vanicek, 1999). Its importance has made it a key target for trying to monitor AABW in the recent past and on glacial-interglacial timescales (eg. Hogg & Zenk, 1997; Ledbetter, 1986; Zenk & Morozov, 2007).

In a series of papers spanning a decade, Ledbetter and co-workers investigated the mean grain size of the silt (4-63 μm) fraction in sediment cores from the Vema Channel, with the aim of identifying changes in flow speed between the Holocene and the LGM (Ledbetter & Johnson, 1976; Ledbetter, 1979, 1984, 1986). Two papers (hereafter LJ76 (Ledbetter & Johnson, 1976) and L84 (Ledbetter, 1984)) presented time slices from suites of cores on the eastern side of the channel with conflicting conclusions. LJ76 argued for an increase in the transport volume of AABW through Vema Channel during the glacial period, whereas L84 argued for the opposite.

However, the data presented in the two studies are consistent and taken together provide some insight into glacial-interglacial changes in flow speed (Fig 2). It appears that there was a general reduction in grain size at depths between 1500 and 4000 m in the glacial period compared to the Holocene. In LJ76 (diamonds), multiple cores from within the deep, central part of the channel showed sharp increases in mean grain size in both the Holocene and the glacial period, occurring at depths between 4111 and 4300 m. Discounting one sample due to an age model error (Ledbetter, 1984), the rapid increase in grain size was found at least 70 m shallower during the glacial period (black diamonds) compared to the Holocene (grey diamonds). The later paper (L84, circles) contained only one glacial sample from comparable depths (4104 m) and this glacial sample did not show an abrupt increase in grain size. However, this result is consistent with data from LJ76 (Fig. 2). Taken together, these papers suggest that glacial flow speed was more sluggish than during the Holocene above 4000 m, with similar rapid speeds in the deep channel and a possible small expansion (~100 m shoaling) of this fast-flowing current to shallower depths.

However, since these papers were published, it has become standard practice to measure sortable silt (i.e. the 10-63 μm fraction, $\widehat{\boldsymbol{SS}}$) as opposed to mean silt grain size. This is due to the tendency of particles <10 μm to exhibit cohesive behaviour, which can affect the sensitivity of mean silt grain size to bottom current strength (McCave & Hall, 2006). In addition, LJ76 and L84 did not remove opal during sample preparation, a part of modern practice that helps to remove grains which may not have been sorted by bottom flow speed processes alone (McCave & Hall, 2006).

Here, we update the results of the Ledbetter papers by analysing $\widehat{\boldsymbol{SS}}$ in a subset of the same cores and in additional cores from the Vema Channel and the Brazil margin (Santos Plateau). Using our new data, we re-evaluate the differences between deep South Atlantic flow in the glacial period and the Holocene. Moreover, the interpretation presented in LJ76 that there was only a 100m shoaling of the boundary between NADW and AABW in the glacial South Atlantic is difficult to reconcile with the many subsequent studies that have revealed the strong glacial Atlantic chemocline at ~2500m (suggestive of a substantial shoaling of NADW) in the glacial Atlantic. We therefore update the interpretation of grain size data from the South Atlantic in the light of more recent paleoceanographic research.

2 Methods

Sediment samples were taken from a variety of cores in the Vema Channel and on the Brazil Margin (Table S1). Holocene and glacial samples were selected from each core by reference to published age models, oxygen isotope stratigraphy and percent carbonate records (Curry & Oppo, 2005; Hoffman & Lund, 2012; Jones, Johnson & Curry, 1984; Ledbetter, 1979, 1984; Lund et al., 2015; Tessin & Lund, 2013).

Age models for cores from the Brazil Margin are based on radiocarbon dating, except for KNR159-113-JPC, KNR159-115-GGC and KNR159-120-GGC. For these cores, samples were taken to match the depths identified as Holocene and glacial using oxygen isotopes based on the studies of Curry and Oppo (2005) and Hoffman and Lund (2012). Given the radiocarbon age models, our Holocene samples range in age from 0-10,900 years, and glacial samples from 18,000-23,000 years, thereby avoiding Heinrich Stadial 1 (Table S1). Some of the Brazil Margin cores contain significant age reversals of several thousand years that may indicate burrowing (Lund et al., 2015). These depths were avoided when sampling. We note that the deeper Brazil Margin cores have tops that are >5000 years old. Interpretation of the deepest samples as representative of the whole Holocene may be complicated by early Holocene changes in the

AMOC (eg. Hoogakker et al., 2011). However, modern AMOC was likely established by ~7 ka and Holocene changes since then have likely been modest.

One core from the Vema Channel (NI-107-09-119-GGC) has radiocarbon data. For the remaining cores, Holocene and glacial samples were selected based on records of percent carbonate in Ledbetter (1979) and Jones et al. (1984) (e.g. Fig. S1). For these data, it is difficult to exclude the possibility that we have sediment outside the 18-23 kyr period above (e.g. samples from early HS1). Additional core-top samples were analysed for comparison of our measurements with those of LJ76 and L84. These core tops were identified as Holocene in age using the above methods (Ledbetter, 1984).

Samples were processed for sortable silt analysis using standard procedures (McCave, Manighetti & Robinson, 1995). In summary, all samples were freeze-dried and weighed prior to disaggregation and wet sieving through 63 μm sieves to remove the coarse fraction. Fines were dried at 40 ^{o}C, and acidified twice in 2 M acetic acid to remove the carbonate fraction. Opal was removed by treatment with 200 ml 2 M $NaCO_{3(aq)}$ at 85 ^{o}C for 5 hours. Samples were stirred during heating after 1 and 4 hours. Between each chemical step, samples were left to settle before the liquid was siphoned. Samples were rinsed between each step with 18 MΩcm water. After treatment samples were stored in 0.2 % 'Calgon' (sodium hexametaphosphate) solution.

$\widehat{\boldsymbol{SS}}$ analysis was conducted using a Coulter Counter Multisizer 4 at Cardiff University. Samples were disaggregated by rotation for ~24 hours and were ultrasonicated for 2 minutes immediately prior to analysis. Aliquots for analysis were taken using a pipettor held to the same depth within the sample vial, following 10 seconds of manual shaking. Particle concentration in the analysis vial was 1.5-4 %. The stirrer speed was set to 35, and a Beckman Enhanced Performance, Multisizer™ 4 beaker used to maintain the sediment in suspension. 70,000 particles were counted per measurement and $\widehat{\boldsymbol{SS}}$ calculated online from the sediment size distribution profiles using the Multisizer4 software. On each day before analysis, the instrument was calibrated using Beckman Coulter L20 aperture instrument calibrator. Most samples were analysed two or three times, using different aliquots (Table S1). The uncertainty on a single measurement is ~±0.1 μm (2 sigma). For samples with repeat measurements we calculated 2 standard errors ranging from ±0.02-0.5 μm (Table S1).

In Section 4 we make use of a recent calibration study (McCave, Thornalley & Hall, 2017) to assess changes in flow speed using the $\widehat{\boldsymbol{SS}}$ proxy. The calibration includes the core top samples measured in this study, and therefore should be appropriate for the estimations here.

3 Results

3.1 Core-top comparison with previous studies

We compared seven core top samples with measurements made in LJ76 and L84 (Fig. 3) the results of which are also included in McCave et al. (2017). The $\widehat{\boldsymbol{SS}}$ results were proportional to the earlier studies' grain size measurements, with only minor scatter (R^2 = 0.97). Implications of this result for data interpretation are discussed in Section 4.2.

3.2 Brazil margin/Santos Plateau

With the exception of the sample at 3350 m, the Holocene Brazil Margin samples have similar $\widehat{\boldsymbol{SS}}$ at all depths, and not much structure can be discerned beyond the uncertainties of the methods (Fig. 4 a,e). The two slowest inferred current speeds are at 4000 m and 3600 m, although these are separated by a depth of relatively high $\widehat{\boldsymbol{SS}}$ at 3950 m. One depth (3350 m) has very high Holocene $\widehat{\boldsymbol{SS}}$ recorded in two samples. The volume distributions of sediment size in both samples were relatively flat, suggesting poorly-sorted sediment. This core site lies on a small rise (80 m high) at the base of a long and relatively steep slope. It is possible that these sample depths are turbidite layers, and are thus discarded in further discussion.

During the glacial period the shallowest three sites on the Brazil margin appear to have had slightly elevated $\widehat{\boldsymbol{SS}}$ relative to the Holocene (Fig. 4 a,e). Below these depths (>2600 m) the glacial $\widehat{\boldsymbol{SS}}$ converge with values from the Holocene. In contrast to the Holocene there are no extreme values of $\widehat{\boldsymbol{SS}}$ at 3350 m. Below this depth, Holocene and LGM $\widehat{\boldsymbol{SS}}$ are similar within uncertainty, with overlapping ranges of inter-sample $\widehat{\boldsymbol{SS}}$.

3.3 Vema Channel

Prior to outlining the results for the cores in Vema Channel it is noted that, when quoting water depths in comparison between glacial and Holocene cores, this is with reference to the eastern side of the channel only (i.e. sites where we have data for both time intervals). Samples shallower than 4 km from the Vema Channel have significantly lower $\widehat{SS}$ (~17-19 μm) than the sites on the Brazil margin (~20-23 μm), which may be due to changing proximity to the sediment source (Fig. 4 b,f). In the Holocene, Vema $\widehat{SS}$ increases dramatically below depths of ~4200m. In L84 and LJ76, the depth of this increase falls between 4184-4235 m. Our studies are therefore consistent in this respect. The Holocene profile of $\widehat{SS}$ in our study increases in a small jump below 3934 m to a maximum of ~20.5 μm close to the upper edge of the eastern plateau of the Vema Channel, a feature that is not seen in the data of LJ76 or L84.

The glacial profile of $\widehat{SS}$ has lower $\widehat{SS}$ for all depths shallower than 3965 m compared to the Holocene (Fig. 4 b,f), also consistent with LJ76 and L84. Glacial $\widehat{SS}$ exhibits an abrupt jump to Holocene-like values at 3965 m, and this sharp increase continues to the two deepest core sites (located at 4148 m and 4181 m on the eastern plateau), which had high $\widehat{SS}$ values (~24 μm) during the glacial period. These values of $\widehat{SS}$ were 3-5 μm greater than the Holocene values at the same sites, and are similar to Holocene sites lying in the deep channel itself. By contrast, L84 (who's samples were from the same transect of the channel) did not observe a glacial increase in grain size in the deepest samples, but did not measure samples deeper than 4104 m. Samples from LJ76 show an increase at 4111 m, 100 m deeper than the shallowest increase observed in our study, but consistent with the largest increase in $\widehat{SS}$ we observe.

4 Discussion

4.1 Changes in Glacial North Atlantic Intermediate Water

Profiles of $\delta^{13}C$, Cd/Ca and radiocarbon in the Atlantic suggest that the glacial water column was divided into Glacial North Atlantic Intermediate Water (GNAIW) above ~2500 m and southern-sourced water below it (eg. Curry & Oppo, 2005; Lynch-Stieglitz et al., 2007), although recent neodymium isotope measurements suggest that a significant portion of the deep water may have been northern-sourced (Howe et al., 2016). Nevertheless, evidence from Pa/Th measurements and $\widehat{SS}$ from the North Atlantic suggests that overturning circulation within the GNAIW was vigorous (Evans & Hall, 2008; Gherardi et al., 2009; Lippold et al., 2016; Thornalley et al., 2013). Our $\widehat{SS}$ data from the Brazil margin tentatively support a strong local flow of GNAIW within the South Atlantic. The shallowest three samples are perhaps shallow enough to have felt the influence of GNAIW during the LGM (Curry & Oppo, 2005), and suggest a mildly strengthened flow above 2500 m. Based on a recent $\widehat{SS}$ calibration, this increase may have been around by ~1-2 cms^{-1} compared with the Holocene (McCave, Thornalley & Hall, 2017). However, we note that this change may not reflect the production rate of GNAIW, but may be controlled by more local processes such as the response of the circulation to local isopycnal forcing or to changes in eddy kinetic energy.

For deeper Brazil Margin samples, the glacial and Holocene $\widehat{SS}$ values are within uncertainty (except for the extreme Holocene $\widehat{SS}$ at 3350 m), suggesting that flow speeds on the deep western boundary were no different between the two periods. This finding is perhaps unexpected given data suggesting a shoaling of the boundary between AABW and GNAIW to ~2500 m (eg. Curry & Oppo, 2005; Hoffman & Lund, 2012). Based upon these studies one might expect slower glacial flow below 2.5 km until the core of AABW is reached. However, recent studies based on neodymium isotopes and data/model assimilation have called the extent of such shoaling into question (Gebbie, 2014; Howe et al., 2016). In addition, we note that, in core sites from 3.5-4 km depth in the Vema Channel, glacial $\widehat{SS}$ was lower than that in the Holocene, in contrast to sites at similar depths on the Brazil Margin. The differences in these results highlight the effects of localised flow speed changes on $\widehat{SS}$. For instance, at depths >3 km, the Brazil Margin becomes the Santos Plateau, a relatively enclosed basin subject to recirculation of major ocean currents (McDonagh, Arhan & Heywood, 2002). Therefore, inferences regarding large scale ocean currents are difficult to make at these depths. The Vema Channel data may represent a more robust estimate of the flow speeds at depths 3.5-3.8 km, and do suggest more sluggish flow, possibly indicative of the boundary between northward flowing AABW and southward flowing GNAIW.

4.2 Changes in AABW strength

Inferences on past changes in AABW flow through Vema Channel are complicated by the relatively complex flow and hydraulic models of this region. Today, AABW (defined loosely as water <2 ^{o}C (Hogg et al., 1982)) is situated below ~3500 m in the Vema Channel, and below ~3300 m over the Santos plateau (Fig. 1). A level of no-motion at ~3700 m in the Vema Channel indicates the modern boundary between northward-flowing AABW and southward-flowing North Atlantic Deep Water (NADW) (Zenk & Visbeck, 2013). The channel itself is divided into a deep central channel (4500-4200 m), a relatively flat eastern plateau (4200 m) and the upper channel. In the deep channel (Figs. 1, 4b, 5), current meters and early grain size measurements (LJ76) have shown that there is currently a very strong northward flow (30 cms^{-1}), generated as a large volume of northward-flowing AABW is focussed into the channel confines (Frey et al., 2017; Hogg et al., 1982). There are two main models (Hogg, 1983; Jungclaus & Vanicek, 1999) for how the flow evolves in the channel, and we discuss the major processes here so that we can analyse the observed changes in $\widehat{\boldsymbol{SS}}$ (Fig. 5).

As AABW accelerates in the Vema channel, the fluid maintains geostrophic balance via an eastward dip of isopycnals. In addition, friction causes a westerly Ekman flow on the channel floor, particularly in the deep channel where flow speeds are high. This flow causes downwelling on the western side, and upwelling on the eastern side of the channel (Fig. 5). Isopycnals dip to the west in the deep channel and a strong thermocline develops on the eastern side. This vertical compression of parcels of water drives an increase in positive relative vorticity, resulting in increased northward flow on the eastern side of the deep channel. In the hydraulic model of Hogg (1983), this velocity increase achieves geostrophic balance through an increased eastward dip of the isopycnals of the overlying layers, resulting in vertical stretching of those layers over the eastern plateau. This stretching causes an increase in negative potential vorticity and a weak southward flow over the plateau, that is observed by current meters and consistent with recent numerical modelling efforts (Frey et al., 2017; Hogg et al., 1982; Hogg, 1983). In both models, the critical point appears to be the change in bathymetric slope at the edge of the plateau where the isotherms and isopycnals are concentrated by frictional or hydraulic processes. However, the high velocity in the deep channel likely extends onto the lowest part of the plateau (Jungclaus & Vanicek, 1999; Ledbetter & Johnson, 1976). We now discuss our results in the context of this model of the flow.

The Holocene $\widehat{SS}$ profile from Vema Channel displays its lowest values from 3600-4000 m, closely corresponding to the modern boundary between NADW and AABW (Zenk & Visbeck, 2013). A small step to higher values at ~4000 m appears as the cores approach the level of the plateau (Fig. 4 b, d). This change in grain size may be related to local changes in slope as much as to focussing of flow through Vema Channel.

The glacial $\widehat{SS}$ profile suggests that, in general and above 3965 m, flow in the Vema Channel region was more sluggish than the Holocene (by ~1-2 cms^{-1}), supporting inferences based on Pa/Th measurements (Gherardi et al., 2009) and perhaps still corresponding to the boundary between AABW and GNAIW (see above). By contrast, glacial $\widehat{SS}$ displays a sharp increase with depth beginning at 3965 m, observed in core sites located on the upper edge of the eastern plateau (Fig. 4 b,f). The initial increase in grain size occurs at the same depth as the small Holocene increase at ~4000 m. Glacial $\widehat{SS}$ values were greater than Holocene values below at least 4148 m depth in the two samples located on the main part of the eastern plateau. These data suggest that flow speeds were ~4-6 cms^{-1} faster during the glacial period in the lower part of the Vema Channel. We note that none of our core sites lie within the deep channel, with the deepest being situated on the lower part of the plateau.

Greater glacial flow speed on the eastern plateau may imply a faster flow of AABW at depths >3965 m, via two possible mechanisms. Firstly, an increase in total flow through the Vema Channel may have outweighed recirculation over the eastern plateau, resulting in fast northward flow on the plateau as well. For example, the sample with the greatest $\widehat{SS}$ value on the plateau is in a small channel, which may have acted in a similar way to the deep Vema Channel, focussing the overall increase in northward flow. Alternatively, a faster flow in the deep channel could have resulted in more intense stretching of water parcels over the plateau, causing an increase in the southward recirculation.

Our glacial period core transect does not extend deeper than ~4200 m and therefore we can only confidently infer faster glacial flow speeds between ~4000 m and 4200 m on the eastern plateau. However, one glacial data point from LJ76 located on the western slope of the deep channel suggests an increase in flow speed there (Ledbetter & Johnson, 1976). Given the correlation between the core-top silt-mean grain size data of LJ76 and our $\widehat{SS}$ data in Figure 3, the glacial value would be ~3 μm greater than the Holocene value if converted to $\widehat{SS}$. This increase is similar in magnitude to the increases we observe on the eastern plateau, suggesting a general increase in glacial flow speed of ~4 cm^{-1} in the deeper Vema Channel, which is 10 % of the maximum flow speed recorded by current meters in the channel. However, detailed comparisons of LJ76 silt (4-63 μm) data with our new $\widehat{SS}$ (10-63 μm) glacial data are not conducted, nor likely justified, because of the potential for changes in the sedimentation of fine sediment (which behaves cohesively and is therefore not current-sorted) and opal in the Atlantic during the glacial period, neither of which were excluded or removed from the LJ76 grain size analyses (Bacon, 1984; McCave & Hall, 2006).

Further tentative evidence for faster glacial flow speeds in the deep channel at depths greater than 4200 m comes from the inability of LJ76 to identify the LGM using oxygen isotope stratigraphy in cores from the deep channel (>4200 m), which they suggest is due to non-deposition or erosion of sediment under fast glacial currents. More effective sediment scouring from the deep channel provides additional support for the idea that the grain size data indicate broadly faster flow in the deepest parts of the Vema channel during the glacial period.

In contrast to the Holocene-LGM differences seen at Vema Channel, $\widehat{SS}$ measurements on the Santos plateau show that mean flow speed at AABW depths was identical within uncertainty between the Holocene and the LGM. AABW enters the Santos Plateau (Fig. 1) from the northern end of the Vema Channel as a sluggish cyclonic circulation (~1-5 cms^{-1}) (McDonagh, Arhan & Heywood, 2002). Therefore, the $\widehat{SS}$ results suggest that AABW flow was similarly sluggish there during the LGM. Due to the recirculatory nature of the flow over the Santos plateau, it is likely a poor indicator of wider changes in AABW flow speed. The Holocene-glacial period changes in AABW flow may be observed in the Vema Channel due to the concentration of the flow there.

On balance, the available data suggest increased northward flow of AABW in the deep Vema channel during the last glacial period. This result suggests that an increase in bottom water flow from the Southern Ocean may have been the cause of the large radiocarbon gradient observed between bottom- and overlying deep-water (Burke et al., 2015). Such an increase in AABW transport was likely at least partly responsible for maintaining the large volume of southern-sourced deep-water in the Atlantic.

Enhanced flow of AABW may have been caused by several factors, including the increased density of glacial AABW driving stronger geostrophic flow, or a greater production rate of AABW due to increased sea-ice production and brine rejection (Adkins, McIntyre & Schrag, 2002; Miller et al., 2012). Alternatively, an increase in glacial deep-ocean stratification - caused by the high salinity of bottom waters – likely led to reduced mixing of AABW with overlying waters in the Southern Ocean, which are rapidly mixed today due to the interaction of the fast-flowing ACC with rough bottom topography (Watson and Naveira Garabato, 2006). Therefore, a greater proportion of AABW may have escaped the Southern Ocean to enter ocean basins to the north, including the Atlantic (Watson and Naveira Garabato, 2006). Such an increase in supply of dense bottom water to the Atlantic may have led to more rapid flow through the Vema Channel and is thus supported by our data.

Because of the importance of deep ocean circulation and AABW production rates in altering past global climate and the carbon cycle, further work is required to investigate the suggestion of this study for enhanced glacial AABW flow, and its relationship to AABW properties and production rate. This may be achieved though the combined use of paleoceanographic proxies containing information on water transport rates, such as ^{14}C, $\widehat{\boldsymbol{SS}}$ and Pa/Th, and the coupling of water mass distribution proxies with inverse modelling techniques (eg. Gebbie, 2014; Lund, Adkins & Ferrari, 2011).

5 Conclusions

We have revisited grain size analyses of sediment cores from the Vema Channel to investigate glacial paleo-flow speed by comparison with Holocene sediments. We used modern methods (sortable silt mean grain size), and expanded the sample set to include sites from the Brazil margin over the Santos Plateau. Our results are broadly consistent with the earlier work of Ledbetter and co-workers.

The results suggest that, during the LGM, intermediate South Atlantic Ocean circulation on the western boundary (shallower than 2600 m) was slightly more vigorous than the Holocene, whereas in general, below 2600 m, inferred flow speeds were similar to the Holocene. However, local recirculation might affect these deeper flow speeds, and so these samples are difficult to use as proxies for the large-scale ocean circulation.

In the Vema Channel, glacial flow speeds were slower than the Holocene at depths shallower than 3965m, possibly representing the boundary between AABW and GNAIW. In contrast, we record increased glacial flow speeds at depths greater than 3965m, located over the eastern plateau of the Vema Channel. Combined with additional data from early studies, we infer that this increase may have resulted from an increase in northward velocity in the deep channel related to increased AABW flow. However, due to the complexity of the circulation within Vema Channel, further hydraulic modelling is ideally required to test the validity of this interpretation of the grain size data. An increase in AABW flow through the Vema Channel may reflect changing mixing rates in the Southern Ocean, and may have helped to sustain the large volume of southern-sourced deep-water in the Atlantic during the glacial period.

Acknowledgments

We would like to thank Ellen Roosen (WHOI) and Nichole Anest (LDEO) for providing samples; Janet Hope (UCL) and Lindsey Owen (Cardiff) for laboratory assistance; and Ian Hall for facilitating grain size analyses at Cardiff University. We thank Andrea Burke for useful discussion on initial results. The project was designed by DJRT, and conducted by PTS and PE. All authors contributed to the discussion and interpretation of results. The manuscript was written by PTS, with contributions from DJRT. Funding was provided as part of the MSc program at UCL for PE, and a Philip Leverhulme Prize to DJRT from the Leverhulme Trust. All data is included as one Table in the supporting information.

References

Adkins, J. F., McIntyre, K. & Schrag, D. P. (2002). The Salinity, Temperature, and δ18O of the Glacial Deep Ocean. *Science*, *298*(5599), pp. 1769–1773. doi: 10.1126/science.1076252

Bacon, M. P. (1984). Glacial to interglacial changes in carbonate and clay sedimentation in the Atlantic Ocean estimated from 230Th measurements. *Chemical Geology*, *46*(2), pp. 97–111. doi: 10.1016/0009-2541(84)90183-9

Barker, S., Knorr, G., Vautravers, M. J., Diz Ferreiro, P. & Skinner, L. C. (2010). Extreme deepening of the Atlantic overturning circulation during deglaciation. *Nature Geoscience*, *3*(8), pp. 567–571. doi: 10.1038/NGEO921

De Boer, A. M. & Hogg, A. M. (2014). Control of the glacial carbon budget by topographically induced mixing. *Geophysical Research Letters*, *41*(12), pp. 4277–4284. doi: 10.1002/2014GL059963

Burke, A., Stewart, A. L., Adkins, J. F., Ferrari, R., Jansen, M. F. & Thompson, A. F. (2015). The glacial mid-depth radiocarbon bulge and its implications for the overturning circulation. *Paleoceanography*, *30*(7), pp. 1021–1039. doi: 10.1002/2015PA002778

Burke, A. & Robinson, L. F. (2012). The Southern Ocean's Role in Carbon Exchange During the Last Deglaciation. *Science*, *335*(6068), pp. 557–561. doi: 10.1126/science.1208163

Curry, W. B. & Oppo, D. W. (2005). Glacial water mass geometry and the distribution of δ13C of ΣCO2 in the western Atlantic Ocean. *Paleoceanography*, *20*(1), pp. 1–12. doi: 10.1029/2004PA001021

Evans, H. K. & Hall, I. R. (2008). Deepwater circulation on Blake Outer Ridge (western North Atlantic) during the Holocene, Younger Dryas, and Last Glacial Maximum. *Geochemistry, Geophysics, Geosystems*, *9*(3), pp. 1–19. doi: 10.1029/2007GC001771

Ferrari, R., Jansen, M. F., Adkins, J. F., Burke, A., Stewart, A. L. & Thompson, A. F. (2014). Antarctic sea ice control on ocean circulation in present and glacial climates.' *Proceedings of the National Academy of Sciences of the United States of America*, *111*(24), pp. 8753–8758. doi: 10.1073/pnas.1323922111

Frey, D. I., Fomin, V. V, Diansky, N. A., Morozov, E. G. & Neiman, V. G. (2017). New Model and Field Data on Estimates of Antarctic Bottom Water Flow through the Deep Vema Channel. *Doklady Earth Sciences Doklady Akademii Nauk. Pleiades Publishing, Ltd*, *474*(1), pp. 561–564. doi: 10.1134/S1028334X17050026

Gebbie, G. (2014). How much did Glacial North Atlantic Water shoal? *Paleoceanography*, *29*(3), pp. 190–209. doi: 10.1002/2013PA002557

Gherardi, J. M., Labeyrie, L., Nave, S., Francois, R., McManus, J. F. & Cortijo, E. (2009). Glacial-interglacial circulation changes inferred from 231Pa/230Th sedimentary record in the North Atlantic region. *Paleoceanography*, *24*(2), p. PA2204. doi: 10.1029/2008PA001696

Hall, I. R., McCave, I. N., Shackleton, N. J., Weedon, G. P. & Harris, S. E. (2001). Intensified deep Pacific inflow and ventilation in Pleistocene glacial times. *Nature*, *412*(6849), pp. 809–812. doi: 10.1038/35090552

Hayes, C. T., Anderson, R. F., Fleisher, M. Q., Huang, K. F., Robinson, L. F., Lu, Y., Cheng, H., Edwards, R. L. & Moran, S. B. (2015). 230Th and 231Pa on GEOTRACES GA03, the U.S. GEOTRACES North Atlantic transect, and implications for modern and paleoceanographic chemical fluxes. *Deep-Sea Research Part II: Topical Studies in Oceanography*, *116*, pp. 29–41. doi: 10.1016/j.dsr2.2014.07.007

Hodell, D. A., Venz, K. A., Charles, C. D. & Ninnemann, U. S. (2003). Pleistocene vertical carbon isotope and carbonate gradients in the South Atlantic sector of the Southern Ocean. *Geochemistry, Geophysics, Geosystems*, *4*(1), pp. 1–19. doi: 10.1029/2002GC000367

Hoffman, J. L. & Lund, D. C. (2012). Refining the stable isotope budget for Antarctic Bottom Water: New foraminiferal data from the abyssal southwest Atlantic. *Paleoceanography*, *27*(1), pp. 1–12. doi: 10.1029/2011PA002216

Hogg, N., Biscaye, P., Gardner, W. & Schmitz, W. J. (1982). On the transport and modification of Antarctic Bottom Water in the Vema Channel. *Journal of Marine Research*, *40*, suppl.(January), pp. 231–263.

Hogg, N. G. (1983). Hydraulic control and flow separation in a multi-layered fluid with application to the Vema Channel. *Journal of Physical Oceanography*, *13*, pp. 695–708. doi: 10.1175/1520-0485(1983)013<0695:HCAFSI>2.0.CO;2

Hogg, N. G. & Zenk, W. (1997). Long-period changes in the bottom water flowing through Vema Channel. *Journal of Geophysical Research: Oceans*, *102*(C7), pp. 15639–15646. doi: 10.1029/97JC00591

Hoogakker, B. A. A., Chapman, M. R., McCave, I. N., Hillaire-Marcel, C., Ellison, C. R. W., Hall, I. R. & Telford, R. J. (2011). Dynamics of North Atlantic Deep Water masses during the Holocene. *Paleoceanography*, *26*(4), p. PA4214. doi: 10.1029/2011PA002155

Howe, J. N. W., Piotrowski, A. M., Noble, T. L., Mulitza, S., Chiessi, C. M. & Bayon, G. (2016). North Atlantic Deep Water Production during the Last Glacial Maximum. *Nature Communications*, *7*, p. 11765. doi: 10.1038/ncomms11765

Jones, G. A., Johnson, D. A. & Curry, W. B. (1984). High-resolution stratigraphy in late Pleistocene/Holocene sediments of the Vema Channel. *Marine Geology*, *58*(1–2), pp. 59–87. doi: 10.1016/0025-3227(84)90116-

Jungclaus, J. H. & Vanicek, M. (1999). Fractionally modified flow in a deep ocean channel: Application to the Vema Channel. *Journal of Geophysical Research: Oceans*, *104*(C9), pp. 21123–21136. doi: 10.1029/1998JC900055

Ledbetter, M. T. (1979). Fluctuations of Antarctic Bottom Water velocity in the Vema Channel during the last 160,000 years. *Marine Geology*, *33*(1–2), pp. 71–89. doi: 10.1016/0025-3227(79)90133-6

Ledbetter, M. T. (1984). Bottom-current speed in the Vema Channel recorded by particle size of sediment fine-fraction. *Marine Geology*, *58*(1–2), pp. 137–149. doi: 10.1016/0025-3227(84)90120-8

Ledbetter, M. T. (1986). A Late Pleistocene time-series of bottom-current speed in the Vema Channel. *Palaeogeography, Palaeoclimatology, Palaeoecology*, *53*(1), pp. 97–105. doi: 10.1016/0031-0182(86)90040-4

Ledbetter, M. T. & Johnson, D. A. (1976). Increased transport of antarctic bottom water in the vema channel during the last ice age. *Science*, *194*(4267), pp. 837–9. doi: 10.1126/science.194.4267.837

Lippold, J., Gutjahr, M., Blaser, P., Christner, E., de Carvalho Ferreira, M. L., Mulitza, S., Christl, M., Wombacher, F., Böhm, E., Antz, B., Cartapanis, O., Vogel, H. & Jaccard, S. L. (2016). Deep water provenance and dynamics of the (de)glacial Atlantic meridional overturning circulation. *Earth and Planetary Science Letters*, *445*, pp. 68–78. doi: 10.1016/j.epsl.2016.04.013

Lund, D. C., Adkins, J. F. & Ferrari, R. (2011). Abyssal Atlantic circulation during the Last Glacial Maximum: Constraining the ratio between transport and vertical mixing. *Paleoceanography*, *26*(1), p. PA1213. doi: 10.1029/2010PA001938

Lund, D. C., Tessin, A. C., Hoffman, J. L. & Schmittner, A. (2015). Southwest Atlantic water mass evolution during the last deglaciation. *Paleoceanography*, *30*(5), pp. 477–494. doi: 10.1002/2014PA002657

Lynch-Stieglitz, J., Adkins, J. F., Curry, W. B., Dokken, T., Hall, I. R., Herguera, J. C., Hirschi, J. J.-M., Ivanova, E. V, Kissel, C., Marchal, O., Marchitto, T. M., McCave, I. N., McManus, J. F., Mulitza, S., Ninnemann, U., Peeters, F., Yu, E.-F. & Zahn, R. (2007). Atlantic meridional overturning circulation during the Last Glacial Maximum. *Science*, *316*(5821), pp. 66–69. doi: 10.1126/science.1137127

McCave, I. N. & Hall, I. R. (2006). Size sorting in marine muds: Processes, pitfalls, and prospects for paleoflow-speed proxies. *Geochemistry, Geophysics, Geosystems*, *7*(10). doi: 10.1029/2006GC001284

Mccave, I. N., Kiefer, T., Thornalley, D. J. R. & Elderfield, H. (2005). Deep flow in the Madagascar-Mascarene Basin over the last 150,000 years. *Philosophical transactions. Series A, Mathematical, physical, and engineering sciences*, *363*(1826), pp. 81–99. doi: 10.1098/rsta.2004.1480

McCave, I. N., Manighetti, B. & Robinson, S. G. (1995). Sortable silt and fine sediment size/composition slicing: Parameters for palaeocurrent speed and palaeoceanography. *Paleoceanography*, *10*(3), pp. 593–610. doi: 10.1029/94PA03039

McCave, I. N., Thornalley, D. J. R. & Hall, I. R. (2017). Relation of sortable silt grain size to deep-sea current speeds: Calibration of the “Mud Current Meter”. *Deep Sea Research Part I: Oceanographic Research Papers*, *127*, pp. 1-12. doi: 10.1016/j.dsr.2017.07.003

McDonagh, E. L., Arhan, M. & Heywood, K. J. (2002). On the circulation of bottom water in the region of the Vema Channel. *Deep-Sea Research Part I: Oceanographic Research Papers*, *49*(7), pp. 1119–1139. doi: 10.1016/S0967-0637(02)00016-X

Miller, M. D., Adkins, J. F., Menemenlis, D. & Schodlok, M. P. (2012). The role of ocean cooling in setting glacial southern source bottom water salinity. *Paleoceanography*, *27*(3), p. PA3207. doi: 10.1029/2012PA002297

Negre, C., Zahn, R., Thomas, A. L., Masqué, P., Henderson, G. M., Martínez-Méndez, G., Hall, I. R. & Mas, J. L. (2010). Reversed flow of Atlantic deep water during the Last Glacial Maximum. *Nature*, *468*(7320), pp. 84–88. doi: 10.1038/nature09508

Schlitzer, R. (2016). Ocean Data View’. Available at: http://odv.awi.de.

Skinner, L. C. (2009). Glacial – interglacial atmospheric CO2 change: a possible “standing volume” effect on deep-ocean carbon sequestration. *Climate of the Past*, *5*(3), pp. 1259–1296. doi: 10.5194/cpd-5-1259-2009

Skinner, L. C., Fallon, S., Waelbroeck, C., Michel, E. & Barker, S. (2010). Ventilation of the deep Southern Ocean and deglacial CO2 rise. *Science*, *328*(5982), pp. 1147–1151. doi: 10.1126/science.1183627

Skinner, L., McCave, I. N., Carter, L., Fallon, S., Scrivner, A. E. & Primeau, F. (2015). Reduced ventilation and enhanced magnitude of the deep Pacific carbon pool during the last glacial period. *Earth and Planetary Science Letters*, *411*, pp. 45–52. doi: 10.1016/j.epsl.2014.11.024

Speer, K. G., Zenk, W., Speer, K. G. & Zenk, W. (1993). The Flow of Antarctic Bottom Water into the Brazil Basin. *Journal of Physical Oceanography*, *23*(12), pp. 2667–2682. doi: 10.1175/1520-0485(1993)023<2667:TFOABW>2.0.CO;2

Tessin, A. C. & Lund, D. C. (2013). Isotopically depleted carbon in the mid-depth South Atlantic during the last deglaciation. *Paleoceanography*, *28*(2), pp. 296–306. doi: 10.1002/palo.20026.
Thomas, A. L., Henderson, G. M. & McCave, I. N. (2007). Constant bottom water flow into the Indian Ocean for the past 140 ka indicated by sediment 231Pa/230Th ratios. *Paleoceanography*, *22*(4), p. PA4210. doi: 10.1029/2007PA001415

Thornalley, D. J. R., Barker, S., Becker, J., Hall, I. R. & Knorr, G. (2013). Abrupt changes in deep Atlantic circulation during the transition to full glacial conditions. *Paleoceanography*, *28*(2), pp. 253–262. doi: 10.1002/palo.20025

Watson, A. J. & Naveira Garabato, A. C. (2006). The role of Southern Ocean mixing and upwelling in glacial-interglacial atmospheric CO2 change. *Tellus, Series B: Chemical and Physical Meteorology*, *58*(1), pp. 73–87. doi: 10.1111/j.1600-0889.2005.00167.x

Zenk, W. & Morozov, E. (2007). Decadal warming of the coldest Antarctic Bottom Water flow through the Vema Channel. *Geophysical Research Letters*, *34*(14), p. L14607. doi: 10.1029/2007GL030340

Zenk, W. & Visbeck, M. (2013). Structure and evolution of the abyssal jet in the Vema Channel of the South Atlantic. *Deep-Sea Research Part II*, *85*, pp. 244–260. doi: 10.1016/j.dsr2.2012.07.033

Figure Captions:

Figure 1: Core sites and modern ocean conditions across the Brazil margin, Santos plateau and Vema channel. Modern AABW is indicated by water temperatures below the 2 ^{o}C isotherm. Simplified bottom currents are plotted after McDonagh and Heywood (2002). Plotted using Ocean Data View and the World Ocean Atlas 2013 (Schlitzer, 2016). Core locations do not exactly align with bathymetry because it is averaged over the width of the section. For a more detailed view of the relationship between the cores and the bathymetry see Figure 4.

Figure 2: Results of Ledbetter and Johnson (1976) and Ledbetter (1984). Profiles of grain size with depth are plotted using a Loess best fit regression combining data from both studies. Confidence intervals were constructed using a Monte Carlo approach considering measurement uncertainty and assuming a depth uncertainty of ±20 m.

Figure 3: L84 silt mean grain size versus sortable silt ($\widehat{SS}$) measurements from this study. Core top samples are from the topmost centimetre of each core. Error bars indicate the range of $\widehat{SS}$ measured at each site. In most cases error bars are smaller than symbols.

Figure 4: Depth and longitudinal profiles of $\widehat{SS}$ made during this study with bathymetry (The GEBCO_2014 Grid, version 20150318, www.gebco.net) for each site: a), c) and e) Brazil Margin and Santos Plateau; b), d) and f) Vema Channel. Core positions where samples were taken from both the Holocene and the glacial period are plotted in c) and d) with black outlines, and core-top-only sites are plotted with white outlines. Bathymetric profiles in a) and b) are taken from the sections (white lines) shown in c) and d). Holocene and glacial profiles of $\widehat{SS}$ are shown in grey and black respectively in a, b, e, f. Each data point shows the average $\widehat{SS}$ of all measurements made at that depth. The error bars show the range of those measurements. Typical uncertainties on single samples are ±0.1 µm. Profiles of grain size with depth (e and f) are plotted using a Loess best fit regression. 90 % confidence intervals on the lines were constructed using a Monte Carlo approach considering measurement uncertainty and assuming a depth uncertainty of ±20 m. Two Holocene points lying outside the Loess regression confidence intervals in f) were from sites north of the main section of sites.

Figure 5: Circulation schematic for the modern Vema Channel. Circles with crosses (dots) denote currents into (out of) the page. Dashed lines depict isopycnals. Arrows in the deep channel show the direction of Ekman transport induced by bottom friction. Remaining arrows show the changes in relative vorticity (+/- ξ) due to compression or stretching of the water column, and the displacement of the current in the main channel due to these effects.

Figure 1.

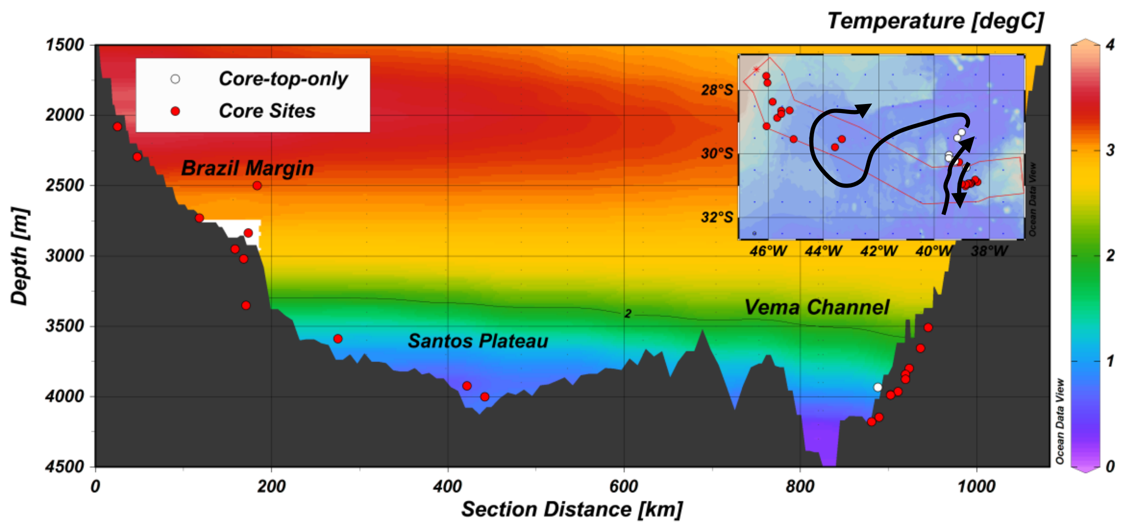

Temperature [degC]
Core-top-only
Core Sites
Brazil Margin
Santos Plateau
Vema Channel
28°S
30°S
32°S
46°W
44°W
42°W
40°W
38°W
Ocean Data View
Depth [m]
1500
2000
2500
3000
3500
4000
4500
0
200
400
600
800
1000
Section Distance [km]
2
4
3
2
1
0
Ocean Data View

Figure 2.

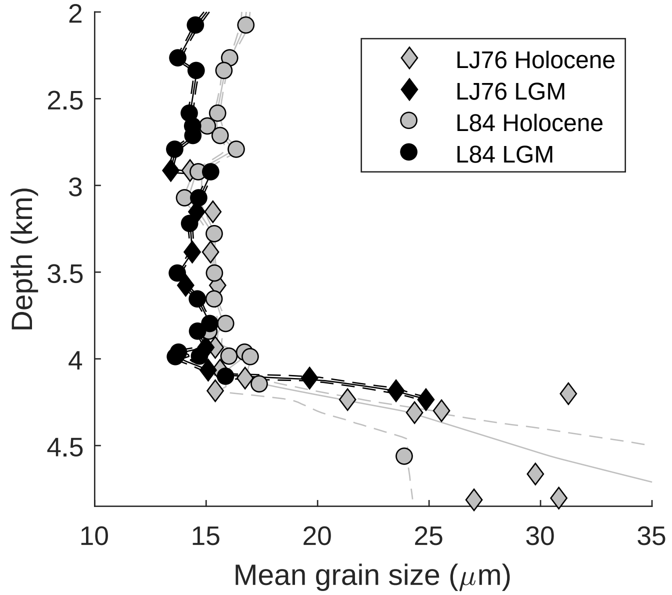

LJ76 Holocene
LJ76 LGM
L84 Holocene
L84 LGM
Depth (km)
2
2.5
3
3.5
4
4.5
10
15
20
25
30
35
Mean grain size (μm)

Figure 3.

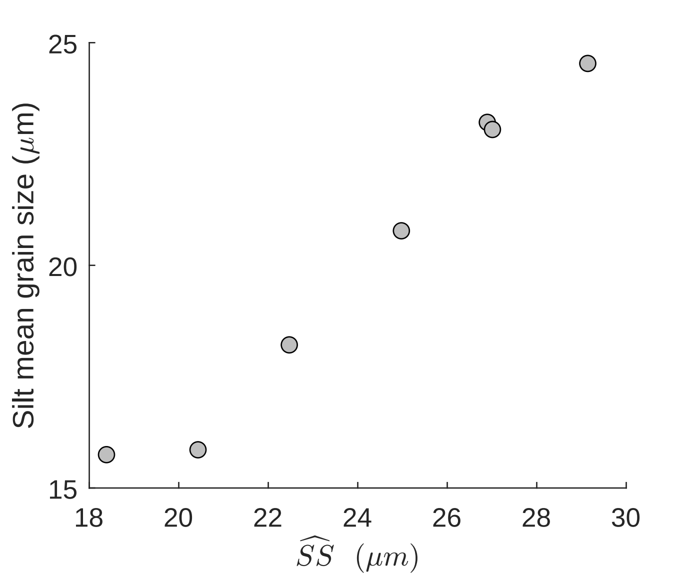
25
20
15
Silt mean grain size (μm)
18
20
22
24
26
28
30
$\widehat{SS}\ \ (\mu m)$

Figure 4.

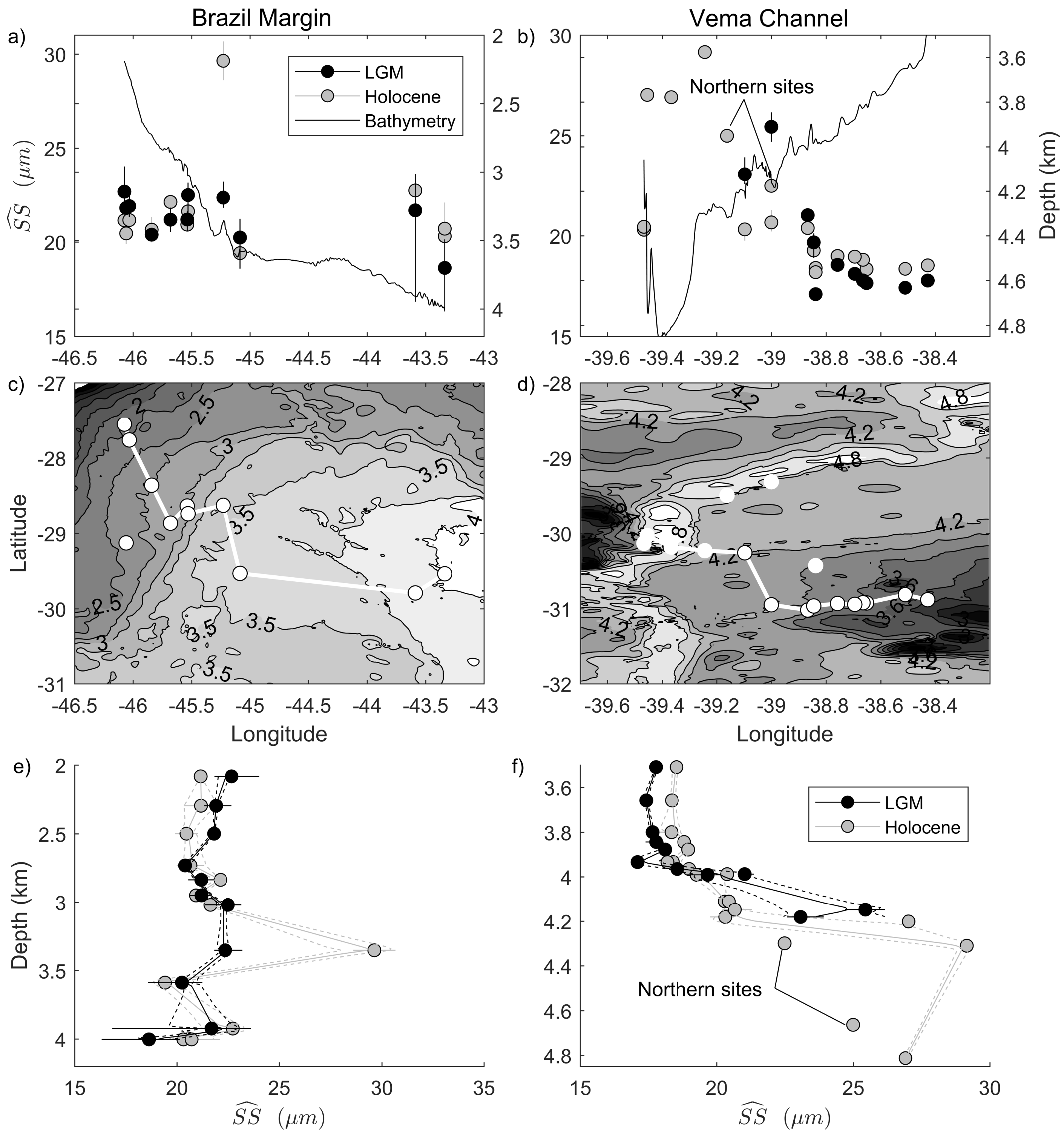

Brazil Margin
Vema Channel
a)
b)
c)
d)
e)
f)
LGM
Holocene
Bathymetry
Northern sites
$\widehat{SS}$ (μm)
Depth (km)
Latitude
Longitude

Figure 5.

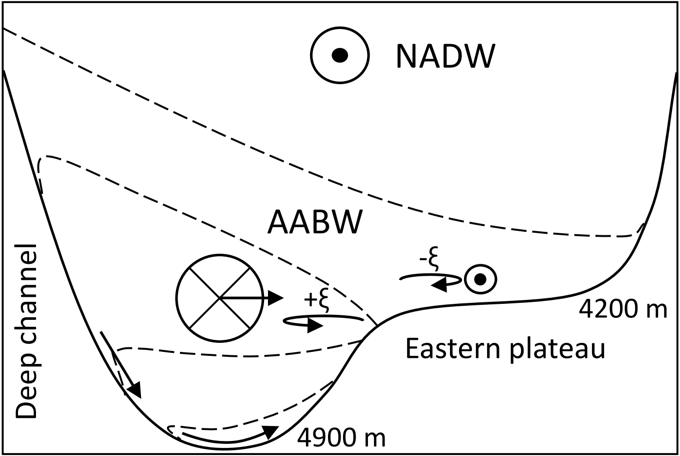
NADW
AABW
-ξ
+ξ
4200 m
Eastern plateau
Deep channel
4900 m